# 1-D imaging of rotation-vibration non-equilibrium from pure rotational ultrafast coherent anti-Stokes Raman scattering

Timothy Y. Chen,[1] Benjamin M. Goldberg,[2] Brian D. Patterson,[2] Egemen Kolemen,[1,3] Yiguang Ju,[1] and Christopher J. Kliewer[2,*]

[1]Department of Mechanical and Aerospace Engineering, Princeton University, Princeton, New Jersey 08544, USA
[2]Sandia National Laboratories, Livermore, California 94551, USA
[3]Princeton Plasma Physics Laboratory, Princeton, New Jersey 08543, USA
*Corresponding author: cjkliew@sandia.gov

**We present one-dimensional (1-D) imaging of rotation-vibration non-equilibrium measured by two-beam pure rotational hybrid femtosecond/picosecond coherent anti-Stokes Raman scattering (fs/ps CARS). Simultaneous measurements of the spatial distribution of molecular rotation-vibration non-equilibrium are critical for understanding molecular energy transfer in low temperature plasmas and hypersonic flows. However, non-equilibrium CARS thermometry until now was limited to point measurements. The red shift of rotational energy levels by vibrational excitation was used to determine the rotational and vibrational temperatures from 1-D images of the pure rotational spectrum. Vibrational temperatures up to 5500 K were detected in a $CH_4/N_2$ nanosecond-pulsed pin-to-pin plasma within 2 mm near the cathode. This approach enables study of non-equilibrium systems with 40 $\mu m$ spatial resolution.**

Rotation-vibration non-equilibrium and energy transfer is a key area of study for low temperature plasmas that enhances chemical reactivity in applications such as materials synthesis [1], plasma catalysis [2], plasma assisted combustion [3], $CO_2$ dissociation [4], and $CH_4$ reforming [5]. Furthermore, rotation-vibration non-equilibrium is critical for understanding the aerodynamics and thermal loading of space vehicles re-entering Earth's atmosphere at hypersonic velocities [6]. In these applications, there exist spatial gradients of temperature due to energy transport across either the boundary layer in hypersonic vehicles [6] or the cathode sheath layer in low temperature plasmas [7]. Therefore, it is of great interest to be able to conduct spatially resolved measurements of rotation-vibration non-equilibrium in these systems. Hybrid femtosecond/picosecond coherent anti-Stokes Raman scattering (fs/ps CARS) is a powerful tool to measure species concentration and temperature on the picosecond time scale and tens of microns

of spatial resolution, while avoiding non-resonant contributions to the CARS spectrum from four-wave mixing [8–16]. This is achieved by generating the Raman coherence through excitation by a spectrally broad femtosecond laser which provides both the pump and Stokes photons. A separate time-delayed spectrally narrow ps pulse scatters off this coherence and generates the CARS signal beam. Since the pump/Stokes and probe beam do not overlap in time, the non-resonant contributions are avoided but many Raman transitions can be probed at once through the broadband excitation.

Typically, simultaneous measurements of rotation-vibration non-equilibrium of molecules like $N_2$ measured by CARS uses the vibrational Q-branch and its rotational structure to determine the rotational and vibrational temperatures [17]. However, the spectral resolution for the fs/ps CARS approach is determined by the spectral width of the ps probe pulse. To resolve the rotational structure, a spectral resolution less than 1 $cm^{-1}$ is required [18,19], which is a major challenge for many fs/ps CARS systems since they use the fs laser to generate ps probe pulses with ∼2 to 3 $cm^{-1}$ resolution [13–15]. As a result of the challenges associated with simultaneous measurements, rotation-vibration non-equilibrium can instead be determined by measuring the rotational S-branch and vibrational Q-branch separately as was done in [20]. However, it is desirable to have simultaneous measurements of rotation-vibration non-equilibrium to understand energy transfer between the rotational and vibrational modes. To overcome the spectral resolution difficulty, a dual-pump CARS scheme was applied for simultaneous measurement of the rotational S-branch and the vibrational Q-branch of $N_2$ and determination of both rotational and vibrational temperatures in a $N_2$ plasma [15]. However, this approach requires four beams, which adds complexity to setup and alignment. More importantly, measurements of the vibrational Q-branch typically require an optical parametric amplifier (OPA) to produce the correct Raman shift in the Stokes beam. This limits the feasible amount of energy in the Stokes beam and makes it difficult to extend the measurement to one-dimensional (1-D) imaging. Therefore, it would be desirable to measure rotation-vibration non-equilibrium using the rotational CARS spectrum instead, where

many photon pairs are available to generate the Raman coherence. Consequently, 1-D imaging is feasible with a 2-beam phase matching scheme [11,12,16]. To our knowledge, only translated point CARS measurements of rotation-vibration non-equilibrium have been done [15,17] and 1-D imaging has not yet been reported.

It has been shown previously that vibrationally excited states of diatomic molecules exhibit a frequency shift in their rotational spectra due to rotation-vibration coupling and can be used as a measure of both rotational and vibrational temperature [21,22]. In fact, vibrational excitation shifts of the rotational levels have been considered for modelling fs/ps rotational CARS measurements of flames and plasmas [15,16]. However, in these fs/ps CARS studies either the rotational modes were assumed to be in equilibrium with the vibrational modes [16] or the probe pulse had insufficient spectral resolution to resolve the vibrational shifts [15]. Furthermore, interfering beat patterns in the time-domain were observed in [15] due to simultaneous sampling of transitions spaced 1 cm$^{-1}$ apart by a probe pulse with ~3 cm$^{-1}$ transform-limited spectral full-width at half maximum (FWHM). As a result, it was argued that dual-pump CARS was needed to determine the rotational temperature in non-equilibrium systems.

In this Letter, we present 1-D two-beam fs/ps CARS imaging of spatial gradients in rotational and vibrational temperatures of $N_2$ in a $CH_4/N_2$ pin-to-pin nanosecond-pulsed discharge near the cathode. We show that with a spectrally narrow picosecond probe pulse, vibrational contributions to the pure rotational CARS spectrum can be directly measured. The required number of beams reduces to two, which simplifies the setup for 1-D CARS imaging.

The theory of fs/ps CARS modelling has been described previously for rotation-vibration equilibrium [10,13] and non-equilibrium environments [15]. Only a brief explanation of the CARS model and illustrative examples of the non-equilibrium spectra will be presented. CARS is a third-order optical non-linear process that utilizes the difference frequency of the pump and Stokes photons to match a resonant molecular rotational or vibrational transition. The time-delayed probe pulse scatters off the coherently excited molecules which generates the CARS signal at the anti-Stokes Raman frequency. In the time-domain, the intensity of the CARS signal can be expressed as follows [10]:

$$I_{CARS}(t) \propto \left| P^{(3)}(t) \right|^2 = \left| \left( \frac{i}{\hbar} \right)^3 E_{pr}(t) \int_0^\infty dt_2 \left( R_{CARS}(t_2) \times \right. \right.$$
$$\left. \left. E_{Stokes}^*(t + \tau_{23} - t_2) \times E_{pump}(t + \tau_{23} + \tau_{12} - t_2) \right) \right|^2 \quad (1)$$

where $P^3(t)$ is the third-order polarization, $E_{pump}$ and $E_{pr}$ are the electric fields of the pump and probe beams, $E_{Stokes}^*$ is the conjugate electric field of the Stokes beam, $\tau_{12}$ is the time delay between the pump and Stokes beams, $\tau_{23}$ is the time delay between the Stokes and probe beams, and $t_2$ is an integration variable representing coherence time scale between the pump/Stokes and the probe beams. The molecular response, $R_{CARS}$, can be written as:

$$R_{CARS}(t) = \sum_v \sum_J I_{v,J \rightarrow v,J+2}$$
$$\times exp \left( \frac{t}{\hbar} \left( i\Delta E_{v,J \rightarrow v,J+2} - \frac{1}{2} \Gamma_{v,J \rightarrow v,J+2}^S \right) \right) \quad (2)$$

where $I_{v,J \rightarrow v,J+2}$ is the Boltzmann-weighted Raman transition intensity modified by the Herman Wallis Factor [23], Placzek-Teller
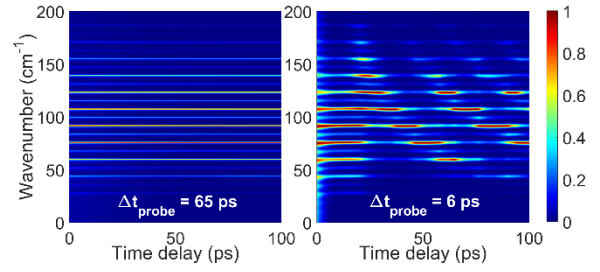


Fig. 1. Modelled time delay scan of $N_2$ rotational CARS spectrum at $T_{rot}$ = 400 K and $T_{vib}$ = 3500 K with a 65 ps probe (left) and a 6 ps probe (right). Coherence beating was only observed for the 6 ps probe.

coefficients, and the polarization anisotropy due to vibrational anharmonicity [24], $\Delta E_{v,J \rightarrow v,J+2}$ is the energy level difference of the rotational S-branch transition, $\Gamma_{v,J \rightarrow v,J+2}^S$ is the Raman linewidth calculated by a Modified Exponential Gap model. Vibrational levels v= 0 to v= 5 were considered and the rotational linewidths were assumed to be the same across all vibrational levels. Rotation-vibration non-equilibrium was considered using a two-temperature Boltzmann distribution similar to [15].

The $N_2$ rotational energy levels were calculated as a function of the vibrational energy level as follows:

$$F(v,J) = B_v \big(J(J + 1)\big) - D_v \big(J^2(J + 1)^2\big) \quad (3)$$

where F is the rotational energy of an $N_2$ molecule in a vibration-rotation state $(v, J)$ while $B_v$ and $D_v$ are the vibrational energy level-dependent rotational and centrifugal constants. $B_v$ and $D_v$ cause red shifts in the rotational energy levels with increasing vibrational energy through rotation-vibration coupling. For molecules in rotation-vibration non-equilibrium, the vibrationally-excited levels cannot be ignored and will appear at these shifted frequencies in the rotational CARS spectrum [21,22]. This enables the detection of rotation-vibration non-equilibrium from pure rotational CARS.

Fig. 1 shows a demonstration of the advantage of using a long ps probe for detection of rotation-vibration non-equilibrium. A time delay scan of the probe pulse with respect to the pump/Stokes beams was simulated for 60 Torr $N_2$ at a rotational temperature, $T_{rot}$ of 400 K and a vibrational temperature, $T_{vib}$, of 3500 K. In Fig. 1, only the duration of the probe pulse was changed from 65 ps (left) to 6 ps (right). With the 65 ps probe, the ~0.23 cm$^{-1}$ spectral width was narrower than the 1 cm$^{-1}$ spacing between adjacent vibrational levels. Each transition was probed separately without any spectral overlap. With the 6 ps probe, beating was observed due to simultaneous sampling of neighboring vibrational levels, cited in [15] to be detrimental for accurate rotational CARS thermometry. The 65 ps probe avoids these effects on the rotational spectrum.

Fig. 2 provides an illustration of the shifted Raman transitions for $N_2$ at a rotational temperature of 500 K and vibrational temperature of 4000 K. The underlying peaks are the vibrationally-shifted rotational Raman transitions simulated with a long probe pulse. The overall profile shown is the total convolution of these peaks with the spectrometer slit function, experimentally fit from room temperature rotational spectra of $N_2$. As seen in Fig. 2, even if the vibrationally-shifted peaks cannot be individually resolved by the spectrometer, their contribution can be determined from the one-sided broadening of the rotational transition. Vibrational broadening can be detected starting from a vibrational temperature of 1500 K and becomes prominent above 2000 K.

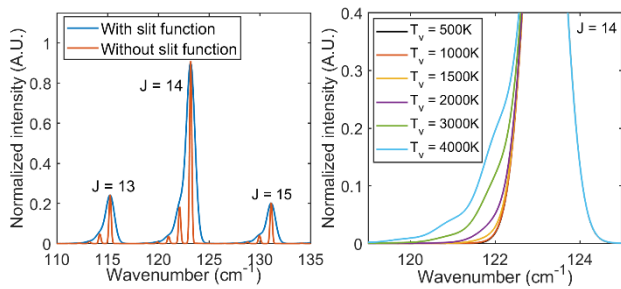The fs/ps CARS setup is shown in Fig. 3 and is similar to the setup

Fig. 2. Modelled non-equilibrium rotational CARS spectra at $T_{rot}$ = 500 K and $T_{vib}$ = 4000 K, with and without convolution with the spectrometer slit function (left). Close up view of the J = 14→16 peak with $T_{rot}$ held at 500 K and $T_{vib}$ varied from 500 K to 4000 K (right).
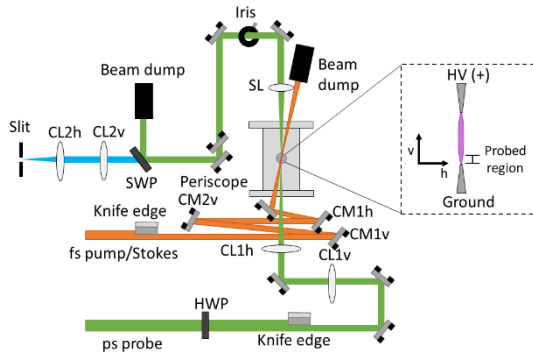


Fig. 3. Experimental setup for fs/ps CARS imaging. CM1h, CM1v, CM2v: concave cylindrical mirrors with f= 400 mm, 400 mm, and 200 mm. CL1v, CL1h, CL2v, CL2h: plano-convex cylindrical lenses with f = 300 mm, 400 mm, 400 mm, 75 mm. SL: spherical plano-convex lens with f = 400 mm. SWP: short wave pass.

in [12]. The 65 ps probe beam was provided by a seeded ps regenerative amplifier that operated at 20 Hz with a pulse energy of 6 mJ. The oscillator of the seed laser for the probe beam was phase-locked to the oscillator of the fs laser with < 1 ps of jitter. The probe delay was controlled electronically (PDL-100A, Colby Instruments). For these measurements and associated simulations, the probe delay was set to 60 ps, which avoided the non-resonant background. The probe beam was focused into a sheet parallel to the electrode gap by a cylindrical lens (f=400 mm). A 1.5 mJ portion of a 1 kHz Ti:Sapphire regenerative amplifier with a pulse width of 50 fs (Legend Elite, Coherent) was split off and focused into a 1 meter long hollow-core fiber with 310 $\mu m$ core diameter filled with 400 Torr of Ar (Kaleidoscope, Femtolasers). The output energy of the hollow-core fiber was 0.6 mJ and the spectral profile of the pulse was significantly broadened by self-phase modulation within the fiber. The spectrally broadened pulse was compressed by negatively chirped mirrors to ~7 fs and was reduced in the vertical dimension (parallel to the electrode gap) by two concave cylindrical mirrors in a 4f configuration (f = 400 mm and 200 mm). Afterward, the fs beam was focused into a sheet by an additional concave cylindrical mirror (f = 400 mm) to serve as the pump/Stokes beam. At the 5° intersection of the two sheets, the CARS signal was produced and propagated with the probe beam. The pump/Stokes beam was sent to a beam dump, while the probe and CARS signal beams were routed through the imaging setup in Fig. 3. The CARS signal was separated from the probe beam by a short-wave pass
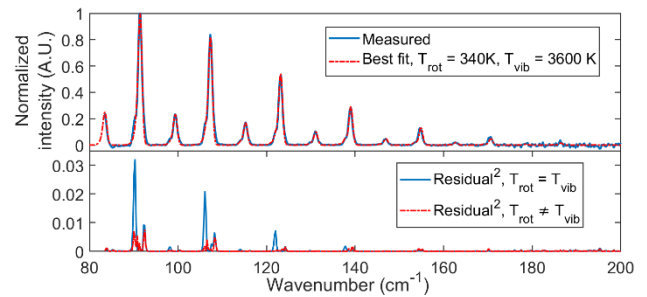
Fig. 4. Example $N_2$ rotation-vibration non-equilibrium fit for a spectrum measured 10 μs after the voltage pulse (top). The squared residuals were plotted for equilibrium and non-equilibrium fits (bottom).

filter (Semrock) and imaged 1:1 onto the 100 $\mu m$ wide slit of the spectrometer (iHR550, Horiba). The CARS signal was dispersed by a 2400 gr/mm grating and was detected by a water-cooled CCD with 13.5 $\mu m$ pixels (Newton 940, Andor). The image exposure time was 2 seconds and 200 images were captured for averaging. Thermal noise was minimized by cooling the CCD to -80°C. The electrodes were machined to 500 $\mu m$ diameter tips and were separated by 1 cm. The 4 kV, 500 ns voltage pulse was supplied by a high voltage switch at 20 Hz (PVX 4130, DEI) triggered by a delay generator (DG645, SRS). The gas mixture used was 40% $CH_4$ and 60% $N_2$ at 60 Torr, and gas was flowed to flush the discharge region between voltage pulses. To measure close to the cathode surface, both the probe and pump/Stokes beams were partially blocked by a knife edge and imaged to the probed region. This created a sharp edge on the incoming beams and reduced light scattering from the cathode surface. The line-spread function was determined by the method in [12] and was ~40 $\mu m$.

All measured spectra were divided by the excitation profile determined from the non-resonant background in pure $CH_4$. The corrected spectra were then fit through nonlinear least-squares fitting based on interpolation of a library of pre-calculated spectra, similar to past fs/ps CARS studies [16]. The fitting parameters were the rotational and vibrational temperatures, and offsets in the baseline intensity and the frequency axis. Bi-linear interpolation was used for the spectral library look-up of the rotational and vibrational temperatures. Shown in Fig. 4 is an example of a fit of a non-equilibrium rotational CARS spectrum with $T_{rot}$= 340 K and $T_{vib}$ = 3600 K. There is a visible "bump" on the low-frequency side of each rotational peak from the higher vibrational levels of $N_2$. The squared residuals were plotted for an equilibrium $T_{rot} = T_{vib} = 340\,K$ fit versus a non-equilibrium $T_{rot} \neq T_{vib}$ fit. At the locations of the expected contributions from the vibrationally excited $N_2$, the residuals show a sharp increase for the equilibrium fit. However, these peaks in the residuals disappear once rotation-vibration non-equilibrium is considered.

It is known from past CARS studies that the vibrational distribution function may not be Boltzmann [15,17]. From Fig. 2, even at vibrational temperatures of 4000 K, vibrational levels higher than v=1 make minor contributions to the spectral profile. Therefore, the reported temperature is the $T_{v01}$ temperature where the ground and first excited vibrational state are used to define the temperature for a Boltzmann vibrational distribution. Since the CARS signal was generated with a spectrally narrow probe pulse, detection of non-Boltzmann vibrational distributions would only require a spectrometer with high enough resolution to differentiate the individual vibrationally-shifted peaks. At best, vibrational levels
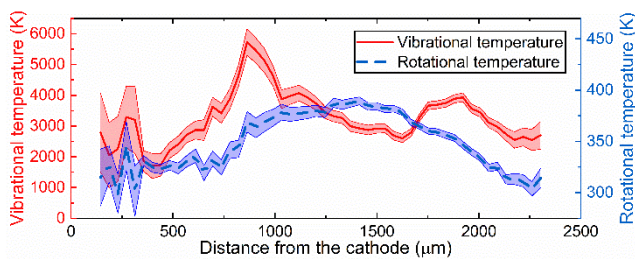
Fig. 5. Spatial distribution of vibrational and rotational temperatures 20 $\mu s$ after the voltage pulse. Error bars are shaded.

up to v = 2 or 3 could be detected with such a spectrometer, while v = 5 was detected with dual-pump CARS [15]. This is because the vibrational Raman cross-section scales with v+1, whereas the rotational Raman cross-section increases by a factor between 1 to 1.5 for v <10 in $N_2$ [24]. The trade-off for higher sensitivity is increased complexity and lower Stokes energy if an OPA is used.

As a demonstration of this method, a 1-D measurement of rotation-vibration non-equilibrium distribution is presented in Fig. 5. The image was taken 20 $\mu s$ after the voltage pulse and three pixel rows were binned post-processing, resulting in ~42 $\mu m$ per point. Error bars were determined based on the 95% confidence intervals of the fits. There was significant rotation-vibration non-equilibrium and spatial gradients in both temperatures, where the peak rotational and vibrational temperatures along the laser sheet were 380 K and 5500 K, respectively. The vibrational temperature exhibited a strong spatial dependence within the first mm of the cathode with a peak at 860 $\mu m$ from the cathode. After the peak, rotation-vibration non-equilibrium remained, and the vibrational temperature was consistently above 2500 K.

In summary, simultaneous measurements of rotation-vibration non-equilibrium in 1-D from pure rotational fs/ps CARS were demonstrated for the first time in a $CH_4/N_2$ nanosecond-pulsed pin-to-pin discharge. The rotation-vibration non-equilibrium was detected using the red shift of the rotational constant with increasing vibrational energy level. This approach enabled the use of two-beam phase matching for straightforward implementation of 1-D imaging with a spatial resolution of 40 $\mu m$. Molecules in non-equilibrium other than $N_2$ can be imaged as well, since only rotation-vibration coupling in the rotational energy levels is required. Measurements in a nanosecond-pulsed plasma showed strong spatial gradients in the rotational and vibrational temperatures starting within 150 $\mu m$ of the cathode surface. The time evolution of the 1-D rotation-vibration non-equilibrium can be obtained by adjusting the electronic delay to the high voltage switch. Such measurements will be the subject of future work. Finally, 2-D measurements of rotation-vibration non-equilibrium may be possible like in equilibrium rotational fs/ps CARS [25] through hyperspectral imaging [26]. This would allow validation of 2-D simulations of non-equilibrium systems critical for development of future plasma technologies and hypersonic vehicles.

## REFERENCES

1. E. Plönjes, P. Palm, G. Babu Viswanathan, V. V. Subramaniam, I. V. Adamovich, W. R. Lempert, H. L. Fraser, and J. W. Rich, Chem. Phys. Lett. **352**, 342-347 (2002).
2. P. Mehta, P. Barboun, F. A. Herrera, J. Kim, P. Rumbach, D. B. Go, J.C. Hicks, and W.F. Schneider, Nat. Catal. **1**, 269-275 (2018).
3. Y. Ju and W. Sun, Prog. in Energy Combust. Sci. **48**, 21-83 (2015).
4. T. Kozák and A. Bogaerts Plasma Sources Sci. Technol. **23**, 045004 (2014).
5. J. Sun and Q. Chen, J. Energy Chem. **39**, 188–197 (2019).
6. I. Armenise, M. Capitelli, G. Colonna, and G. Gorse, J. Thermophys. Heat Tr. **10**, 397-405 (1996).
7. K. Takashima, Z. Yin, and I. V. Adamovich, Plasma Sources Sci. Technol. **22**, 015013 (2012).
8. B. D. Prince, A. Chakraborty, B. M. Prince, and H. U. Stauffer, J. Chem. Phys. **125**, 044502 (2006).
9. D. Pestov, R. K. Murawski, G. O. Ariunbold, X. Wang, M. Zhi, A. V. Sokolov, V. A. Sautenkov, Y. V. Rostovtsev, A. Dogariu, Y. Huang, and M. O. Scully, Science **316**, 265–268 (2007).
10. H. U. Stauffer, J. D. Miller, M. N. Slipchenko, T. R. Meyer, B. D. Prince, S. Roy, and J. R. Gord, J. Chem. Phys. **140**, 024316 (2014).
11. A. Bohlin, B. D. Patterson, and C. J. Kliewer, J. Chem. Phys. **138**, 081102 (2013).
12. A. Bohlin and C. J. Kliewer, J. Phys. Chem. Lett. **6**, 643–649 (2015).
13. S. P. Kearney and D. J. Scoglietti, Opt. Lett. **38**, 833 (2013).
14. K. A. Rahman, E. L. Braun, M. N. Slipchenko, S. Roy, and T. R. Meyer, Opt. Lett. **45**, 503 (2020).
15. C. E. Dedic, T. R. Meyer, and J. B. Michael, Optica **4**, 563 (2017).
16. J. E. Retter, G. S. Elliott, and S. P. Kearney, Combust. Flame **191**, 527-540 (2018).
17. A. Montello, Z. Yin, D. Burnette, I. V. Adamovich, and W. R. Lempert, J. Phys. D **46**, 464002 (2013).
18. M. Pealat, P. Bouchardy, M. Lefebvre, and J.-P. Taran, Appl. Opt. **24**, 1012 (1985).
19. M. Nafa, M. Scherman, A. Bresson, A. Aubin, A. Godard, B. Attal-Tretout, and P. Joubert, Aerospace Lab Journal **12**, 1 (2016).
20. A. Dogariu, L. E. Dogariu, M. S. Smith, J. Lafferty, and R. B. Miles, AIAA SciTech 2019 Forum (2019).
21. J. J. Barrett and A. B. Harvey, J. Opt. Soc. Am. **65**, 392 (1975).
22. R. E. Teets and J. H. Bechtel, Opt. Lett. **6**, 458 (1981).
23. A. Bohlin, P.-E. Bengtsson, and M. Marrocco, J. Raman Spectrosc. **42**, 1843-1847 (2011).
24. M. C. Drake, Opt. Lett. **7**, 440 (1982).
25. A. Bohlin and C. J. Kliewer, J. Chem. Phys. **138**, 221101 (2013).
26. B. K. Ford, M. R. Descour, and R. M. Lynch, Opt. Express **9**, 444 (2001).

# REFERENCES

1. E. Plönjes, P. Palm, G. Babu Viswanathan, V. V. Subramaniam, I. V. Adamovich, W. R. Lempert, H. L. Fraser, and J. William Rich, "Synthesis of single-walled carbon nanotubes in vibrationally non-equilibrium carbon monoxide," Chemical Physics Letters **352**, 342–347 (2002).
2. P. Mehta, P. Barboun, F. A. Herrera, J. Kim, P. Rumbach, D. B. Go, J. C. Hicks, and W. F. Schneider, "Overcoming ammonia synthesis scaling relations with plasma-enabled catalysis," Nat Catal **1**, 269–275 (2018).
3. Y. Ju and W. Sun, "Plasma assisted combustion: Dynamics and chemistry," Progress in Energy and Combustion Science **48**, 21–83 (2015).
4. T. Kozák and A. Bogaerts, "Splitting of $CO_2$ by vibrational excitation in non-equilibrium plasmas: a reaction kinetics model," Plasma Sources Science and Technology **23**, 045004 (2014).
5. J. Sun and Q. Chen, "Kinetic roles of vibrational excitation in RF plasma assisted methane pyrolysis," Journal of Energy Chemistry **39**, 188–197 (2019).
6. I. Armenise, M. Capitelli, G. Colonna, and G. Gorse, "Nonequilibrium vibrational kinetics in the boundary layer of re-entering bodies," Journal of Thermophysics and Heat Transfer **10**, 397–405 (1996).
7. K. Takashima, Z. Yin, and I. V. Adamovich, "Measurements and kinetic modeling of energy coupling in volume and surface nanosecond pulse discharges," Plasma Sources Science and Technology **22**, 015013 (2012).
8. B. D. Prince, A. Chakraborty, B. M. Prince, and H. U. Stauffer, "Development of simultaneous frequency- and time-resolved coherent anti-Stokes Raman scattering for ultrafast detection of molecular Raman spectra," The Journal of Chemical Physics **125**, 044502 (2006).
9. D. Pestov, R. K. Murawski, G. O. Ariunbold, X. Wang, M. Zhi, A. V. Sokolov, V. A. Sautenkov, Y. V. Rostovtsev, A. Dogariu, Y. Huang, and M. O. Scully, "Optimizing the Laser-Pulse Configuration for Coherent Raman Spectroscopy," Science **316**, 265–268 (2007).
10. H. U. Stauffer, J. D. Miller, M. N. Slipchenko, T. R. Meyer, B. D. Prince, S. Roy, and J. R. Gord, "Time- and frequency-dependent model of time-resolved coherent anti-Stokes Raman scattering (CARS) with a picosecond-duration probe pulse," The Journal of Chemical Physics **140**, 024316 (2014).
11. A. Bohlin, B. D. Patterson, and C. J. Kliewer, "Communication: Simplified two-beam rotational CARS signal generation demonstrated in 1D," The Journal of Chemical Physics **138**, 081102 (2013).
12. A. Bohlin and C. J. Kliewer, "Direct Coherent Raman Temperature Imaging and Wideband Chemical Detection in a Hydrocarbon Flat Flame," J. Phys. Chem. Lett. **6**, 643–649 (2015).
13. S. P. Kearney and D. J. Scoglietti, "Hybrid femtosecond/picosecond rotational coherent anti-Stokes Raman scattering at flame temperatures using a second-harmonic bandwidth-compressed probe," Opt. Lett. **38**, 833 (2013).
14. K. A. Rahman, E. L. Braun, M. N. Slipchenko, S. Roy, and T. R. Meyer, "Flexible chirp-free probe pulse amplification for kHz fs/ps rotational CARS," Opt. Lett. **45**, 503 (2020).
15. C. E. Dedic, T. R. Meyer, and J. B. Michael, "Single-shot ultrafast coherent anti-Stokes Raman scattering of vibrational/rotational nonequilibrium," Optica **4**, 563 (2017).
16. J. E. Retter, G. S. Elliott, and S. P. Kearney, "Dielectric-barrier-discharge plasma-assisted hydrogen diffusion flame. Part 1: Temperature, oxygen, and fuel measurements by one-dimensional fs/ps rotational CARS imaging," Combustion and Flame **191**, 527–540 (2018).
17. A. Montello, Z. Yin, D. Burnette, I. V. Adamovich, and W. R. Lempert, "Picosecond CARS measurements of nitrogen vibrational loading and rotational/translational temperature in non-equilibrium discharges," Journal of Physics D: Applied Physics **46**, 464002 (2013).
18. M. Pealat, P. Bouchardy, M. Lefebvre, and J.-P. Taran, "Precision of multiplex CARS temperature measurements," Applied optics **24**, 1012–1022 (1985).
19. M. Nafa, M. Scherman, A. Bresson, A. Aubin, A. Godard, B. Attal-Tretout, and P. Joubert, "Ro-vibrational spectroscopy in hybrid fs/ps-CARS for N 2 thermometry," AerospaceLab Journal (2016).
20. A. Dogariu, L. E. Dogariu, M. S. Smith, J. Lafferty, and R. B. Miles, "Single Shot Temperature Measurements using Coherent Anti-Stokes Raman Scattering in Mach 14 Flow at the Hypervelocity AEDC Tunnel 9," in *AIAA Scitech 2019 Forum* (American Institute of Aeronautics and Astronautics, 2019).
21. J. J. Barrett and A. B. Harvey, "Vibrational and rotational–translational temperatures in N_2 by interferometric measurement of the pure rotational Raman effect," J. Opt. Soc. Am. **65**, 392 (1975).
22. R. E. Teets and J. H. Bechtel, "Coherent anti-Stokes Raman spectra of oxygen atoms in flames," Opt. Lett. **6**, 458 (1981).
23. A. Bohlin, P.-E. Bengtsson, and M. Marrocco, "On the sensitivity of rotational CARS N2 thermometry to the Herman-Wallis factor," J. Raman Spectrosc. **42**, 1843–1847 (2011).
24. M. C. Drake, "Rotational Raman intensity-correction factors due to vibrational anharmonicity: their effect on temperature measurements," Opt. Lett. **7**, 440 (1982).
25. A. Bohlin and C. J. Kliewer, "Communication: Two-dimensional gas-phase coherent anti-Stokes Raman spectroscopy (2D-CARS): Simultaneous planar imaging and multiplex spectroscopy in a single laser shot," The Journal of Chemical Physics **138**, 221101 (2013).
26. B. K. Ford, M. R. Descour, and R. M. Lynch, "Large-image-format computed tomography imaging spectrometer for fluorescence microscopy," Opt. Express **9**, 444 (2001).